961 STATISTICAL RELATIONSHIPS BETWEEN LARGE-SCALE OSCILLATION PHENOMENA AND MESO-SCALE ATMOSPHERIC CONDITIONS OVER CENTRAL/EASTERN EUROPE AND THEIR REPRESENTATION IN CMIP5 GENERAL CIRCULATION MODELS

Erzsébet Kristóf[*1], Rita Pongrácz[1,2], Judit Bartholy[1,2]
[1]Department of Meteorology, Eötvös Loránd University, Budapest, Hungary
[2]Faculty of Science, Excellence Center, Eötvös Loránd University, Martonvásár, Hungary

1. INTRODUCTION

Atmospheric oscillation phenomena or teleconnection systems are large-scale circulation patterns, which can be interpreted as regions with significant positive or negative correlation with each other (American Meteorological Society, 2018). In this study the effects of teleconnection systems are examined over the Carpathian Basin located in Central/Eastern Europe (i.e. 16°E-24°E & 44°N-50°N). First, we aim to assess the spatio-temporal changes of the atmospheric oscillation phenomena over the Northern Hemisphere from the 1950s to the Millennium using statistical methods. Then, statistical relationships between the identified oscillation phenomena and near-surface air temperature over the Carpathian Basin are explored in details. These evaluations are based on the time series of geopotential height at 500 hPa (AT500hPa) from the European Centre for Medium-Range Weather Forecasts' (ECMWF) ERA-20C reanalysis datasets (European Centre for Medium-Range Weather Forecasts, 2014). Similar analyses are carried out on the historical simulations of general circulation models (GCMs) from the Coupled Model Intercomparison Project Phase 5 (CMIP5) (Taylor et al., 2012). Finally, the results of the GCM simulations are compared to the ERA-20C dataset. We aim to evaluate the capabilities of the GCMs to reproduce teleconnection systems identified from the ERA-20C data. Differences between the GCM simulations and reanalysis datasets are evaluated by various metrics (e.g. spatial correlation, root-mean-square error, RMSE) (Taylor, 2001).

Teleconnection method based on correlation analysis can be considered an effective way to explore oscillation phenomena. Previously it was conducted by Wallace & Gutzler (1981) and Barnston & Livezey (1987) over the Northern Hemisphere's geopotential height fields at 500 hPa and 700 hPa, respectively. Barnston & Livezey (1987) applied principal component analysis to detect the North Pacific Oscillation (NPO), the North Atlantic Oscillation (NAO), the Scandinavian Oscillation (SCA), and the East Atlantic/Western Russia (EA/WR) pattern. The role of the NAO in the North Atlantic region is widely studied (e.g. Hurrell et al., 2003, Hurrell & Deser, 2010). Jung & Hilmer (2000) pointed out that an eastward shift can be observed between 1958-1977 and 1987-1997 regarding the longitudinal position of the action centers of the NAO. They examined the statistical relationship between sea level pressure anomalies and winter (DJF) NAO index. Based on these available results, we expect increasing effect of the NAO concerning the climatic conditions of the Carpathian Basin by 2000. Bartholy et al. (2010) examined the connection between the NAO, local air temperature and precipitation in the Carpathian Basin. The study took into account macrosynoptic circulation patterns also. It was pointed out that the positive and negative phases of the NAO affect the Carpathian Basin during wintertime as follows. In general, cold and wet winters occur in negative phases while warm and dry winters are associated with positive phases.

Closer to our target region the Mediterranean Oscillation (MO) was identified (Conte et al. 1989) in the region of the Mediterranean Sea (Mediterranean region). Ciarlo & Aquilina (2015) analyzed the MO over the southern region of Europe indicating significant correlation between the MO and local air temperature/ precipitation.

Because of their relative closeness to the Carpathian Basin, detecting the signals of the NAO and MO is the scope of our study. We choose to investigate teleconnection systems at the middle troposphere in the AT500hPa field where the signals of the NAO and MO are both expected to be identified.

2. DATA AND METHODS

To detect teleconnection patterns, geopotential data series at the pressure surface of 500 hPa from ERA-20C are used for the time periods of 1951-1980, 1961-1990 and 1971-2000. Only winter months (December, January and February, DJF) are selected for the analysis because meso-scale atmospheric processes are especially dominated by large-scale atmospheric circulations in winter. Daily averages are computed from ERA-20C 3-hourly geopotential data. Then, geopotential data are converted to geopotential height. In addition, historical daily geopotential height datasets of the GCMs are available in the CMIP5 simulation database. We compared them to the time series of the ERA-20C. GCMs that are used in this study are listed in *Table 1*.

GCMs with finer than 2°×2° original spatial resolution are analyzed here. The simulation outputs are interpolated to a grid with 2°×2° using bilinear

[*] *Corresponding author address:* Erzsébet Kristóf, Eötvös Loránd University, Department of Meteorology, Budapest, Hungary, e-mail: ekristof86@caesar.elte.hu

interpolation. We chose the same spatial resolution for the ERA-20C datasets.

To reduce seasonality, daily anomaly datasets are used, namely, corresponding multi-year daily averages are subtracted from the daily AT500hPa time series. To get equally long time series in each month for the statistical analysis, the 31st days of December and January, as well as the 29th and – in the case of some GCMs – 30th days of February are omitted. To avoid the detection of spurious correlations, the fitted linear trend is removed by using least square regression.

As a result, time series in every grid point (180×46) consists of 2640 elements (i.e. 30×88), in every 30-year-long time period.

Table 1. List of the applied GCMs, their developers and original spatial resolution (geographical latitude and longitude). Experiment r1i1p1 is used except in the case of CCSM4 (where r6i1p1 is used instead).

No.	Name of the GCM	Institute (Developer)	Spatial resolution
1	ACCESS1-0	Commonwealth Scientific and Industrial Research Organization (CSIRO) and Bureau of Meteorology (BOM), Australia	1.25° × 1.875°
2	ACCESS1-3	Commonwealth Scientific and Industrial Research Organization (CSIRO) and Bureau of Meteorology (BOM), Australia	1.25° × 1.875°
3	CCSM4	National Center for Atmospheric Research (NCAR), United States of America	~0.9424° × 1.25°
4	CMCC-CM	Centro Euro-Mediterraneo per i Cambiamenti (CMCC) (Euro-Mediterranean Center on Climate Change), Italy	~0.74843° × 1°
5	CMCC-CMS	Centro Euro-Mediterraneo per i Cambiamenti (CMCC) (Euro-Mediterranean Center on Climate Change), Italy	~1.8651° × 1.875°
6	CNRM-CM5	Centre National de Recherches Meteorologiques (CNRM), Meteo-France and Centre Europeen de Recherches et de Formation Avancee en Calcul Scientifique (CERFACS), France	~1.40076° × 1.40625°
7	HadGEM2-AO	National Institute of Meteorological Research (NIMR), South Korea	1.25° × 1.875°
8	HadGEM2-CC	Met Office Hadley Centre (MOHC), United Kingdom	1.25° × 1.875°
9	MIROC5	Atmosphere and Ocean Research Institute (AORI), The University of Tokyo and National Institute for Environmental Studies (NIES), Japan Agency for Marine-Earth Science and Technology (JAMSTEC), Japan	~1.40076° × 1.40625°
10	MPI-ESM-LR	Max Planck Institute for Meteorology, Germany	~1.86526° × 1.875°
11	MPI-ESM-MR	Max Planck Institute for Meteorology, Germany	~1.86526° × 1.875°
12	MPI-ESM-P	Max Planck Institute for Meteorology, Germany	~1.86526° × 1.875°
13	MRI-CGCM3	Meteorological Research Institute, Japan	~1.12149° × 1.125°
14	MRI-ESM1	Meteorological Research Institute, Japan	~1.12147° × 1.125°

First, Pearson and Spearman correlations were computed based on the detrended daily anomaly datasets of the ERA-20C and the GCMs. Computing both type of correlations is beneficial because Pearson and Spearman correlations measure the strength of the linear and monotonic relationship between two variables, respectively. Consequently, Spearman correlation can take into account the nonlinear effects of the atmospheric variability. Using teleconnection method, every grid point is correlated with all the other grid points over the Northern Hemisphere. After that the absolute minimum correlation value (i.e. the strongest negative correlation) is selected in each grid point. Locally, grid points with the statistically significant strongest negative correlation coefficients that are in one-to-one correspondence with each other are considered as potential action centers. Local minimum indicates that any other grid point in a given vicinity of the specific grid point does not result in a stronger negative correlation than what is selected.

To decide whether or not correlations are significant, field significance test is conducted applying Monte Carlo method (Livezey & Chen, 1983). First, surrogate datasets are created by randomly reshuffling

the elements of the original time series in the grid points, which are detected as potential action centers. Then, the original time series are replaced with surrogate data series. Finally, correlation fields are computed again using the newly generated data series. If the original correlation values associated with the potential action centers are stronger than those computed on the basis of the original time series and the surrogate datasets, then the originally computed correlations cannot be considered as the results of a random phenomenon at a given significance level. A total of 1000 simulations are made with those surrogate datasets in each potential action center. The results suggest that correlation values below -0.2 can be considered statistically significant at a significance level of 0.01.

3. RESULTS – ACTION CENTERS IN THE ERA-20C

3.1. Identification of the action centers

To get the most reliable results, a pair of grid points with associated correlation value below -0.3 is chosen as a pair of action centers, if it fulfils the following criteria. It has a vicinity of 14° that does not contain any other grid point with stronger negative correlation. If the correlation value is between -0.3 and -0.4 then there has to be at least another pair of grid points closer than 14° that are one-to-one correspondence with each other. (The associated correlation value also has to be below -0.3). Exceptions are grid points with associated correlation values below -0.4.

Based on the above-listed criteria seven pairs of grid points are identified as pairs of action centers during both 1951-1980 and 1961-1990, furthermore, six pairs can be found during 1971-2000 in both the Pearson and Spearman correlation fields (*Figure 1*).

Figure 1. The strongest negative (a) Pearson and (b) Spearman correlations below -0.2 based on ERA-20C data during 1971-2000 (blue shaded grid points) with identified action centers during 1951-1980, 1961-1990 and 1971-2000 (black, gray and red dots linked with same color lines, respectively). Correlation values associated with action centers for the period of 1971-2000 are written with red.

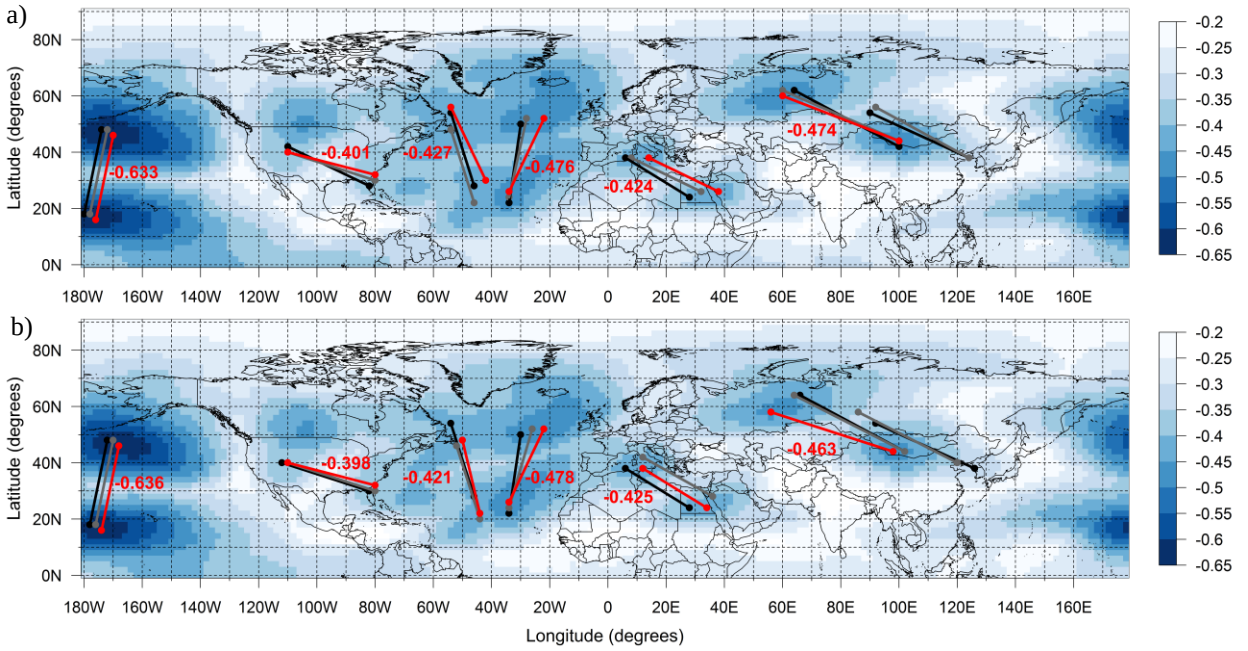

Identified action centers are located above the Pacific Ocean, North America, the Atlantic Ocean, in the Mediterranean region, and above Asia (this list is from west to east). Note that two pairs of action centers are detected over the Northeastern Atlantic region. The first one is located over the western part, and the other one can be found over the eastern part. Similarly, two pairs of action centers are detected above Asia as well. However, only one of them can be identified in the period of 1971-2000.

Identified action centers located over the Atlantic Ocean and the Mediterranean region can be the signals of the NAO and MO, respectively. The location of the action centers are summarized in *Table 2*.

Table 2. Location of the action centers in the ERA-20C based on the strongest negative Pearson and Spearman correlations over the Northeast Atlantic and the Mediterranean region, and the associated correlation values.

Action centers	Period of time	Location based on Pearson correlation	Location based on Spearman correlation	Pearson correlation	Spearman correlation
North-east Atlantic	1951-1980	22°N & 34°W - 50°N & 30°W	22°N & 34°W - 50°N & 30°W	-0.500	-0.506
	1961-1990	24°N & 34°W - 52°N & 28°W	24°N & 34°W - 52°N & 26°W	-0.497	-0.498
	1971-2000	26°N & 34°W - 52°N & 22°W	26°N & 34°W - 52°N & 22°W	-0.476	-0.478
Mediter-ranean	1951-1980	38°N & 6°E - 24°N & 28°E	38°N & 6°E - 24°N & 28°E	-0.438	-0.435
	1961-1990	38°N & 8°E - 26°N & 32°E	42°N & 12°E - 28°N & 36°E	-0.397	-0.404
	1971-2000	38°N & 14°E - 26°N & 38°E	38°N & 12°E - 24°N & 34°E	-0.424	-0.425

3.2. Spatial differences between the action centers in Pearson and Spearman correlation fields

Between the Pearson and Spearman correlation fields the largest difference regarding the location of the action centers is 8° (i.e. 4 grid points). It occurs during 1971-2000. The sum of differences are 22°, 52° and 40° during 1951-1980, 1961-1990 and 1971-2000, respectively. The largest/smallest differences are observed in the case of the action centers over the Northwest Atlantic (30°) / Northeast Atlantic (2°), regardless the time period.

The smallest differences can be observed during the period of 1951-1980. There is no difference over the Northeast Atlantic regarding the types of the correlation. The maximum value of difference is 2° concerning the other six pairs of action centers. The largest difference is 6° during 1961-1990. It can be observed over the eastern part of Asia. As we mentioned above, the largest difference is 8° for the period of 1971-2000; it can be found over the Northwest Atlantic. However, the maximum value of difference is 4° regarding the other five pairs of action centers and there is a perfect matching over North America.

3.3. Changes of the action centers in time

If we compare 1951-1980 and 1971-2000, similar changes can be recognized both in the Pearson and Spearman correlation fields regarding the locations of the action centers. In general, eastward shifts are observed in every case with the exception of Asia.

Concerning the action centers over the Northeast Atlantic, the northern action center moved to an eastern direction (8°) and the southern action center moved northward (4°) in both correlation fields. The eastward shift shown here, reinforces the results of Jung & Hilmer (2000).

Regarding the action centers over the Mediterranean region, remarkable eastward shift is detected comparing 1951-1980 and 1971-2000. Larger shift is observed in the Pearson correlation field (8° and 10° in the case of the western and eastern action centers, respectively) than in the Spearman correlation field (6° and 6°).

A slight decrease (<0.025) can be observed concerning the correlation values associated with the action centers comparing 1951-1980 to 1971-2000. The movements of the action centers through time can be seen in *Figure 1*.

4. RESULTS – VALIDATION OF THE GCMS AGAINST THE ERA-20C

4.1. Distribution of the significant correlation values

To evaluate the GCMs, first, the largest differences between the strongest negative Pearson and Spearman correlation values are compared to each other in the case of each GCM to the ERA-20C.

In the ERA-20C, the largest differences between Pearson and Spearman correlations concerning the same grid point are 0.063, 0.052 and 0.047 in 1951-1980, 1961-1990 and 1971-2000, respectively. The averages of the largest differences regardless the time periods are shown in *Figure 2*. There is only a slight difference between the Pearson and Spearman correlations calculated from the simulation outputs of models MPI-ESM and HadGEM2-CC, similarly to the ERA-20C database.

Small differences between Pearson and Spearman correlations in the ERA-20C indicate that we cannot detect significant nonlinear effect concerning the AT500hPa field by computing Spearman correlation, while there are remarkable differences in some models (e.g. CCSM4, CNRM-CM5).

Figure 2. The largest differences between Pearson and Spearman correlation values based on the GCMs and the ERA-20C data. Averages were computed over the three periods of time (1951-1980, 1961-1990, 1971-2000). Differences between the GCMs and the ERA-20C that are smaller than 0.01 (in absolute value) are framed.

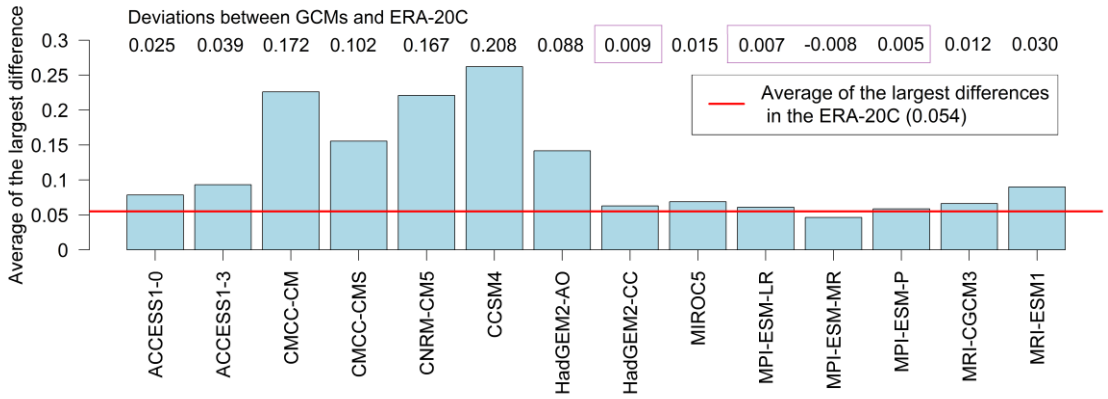

The North Atlantic/European region (14°N-70°N & 90°W-90°E) is analyzed in the rest of this paper. The selection can be explained by the fact that the action centers representing the NAO and MO (possibly infuencing the climatic conditions of the Carpathian Basin) can be found in this area. Over that area the ratio of significant strongest negative correlations (<-0.2) reach 95%. The largest differences between Pearson and Spearman correlations over the target region in the case of the HadGEM2-CC and MPI-ESM are similarly small as in the ERA-20C.

As the second step of the validation, the spatial distribution of the correlation fields of the GCMs are compared to the ERA-20C applying Taylor diagrams (Taylor, 2001). Taylor diagrams of the average values are shown in *Figure 3*.

Concerning the strongest negative Pearson and Spearman correlations, their average value over the three periods of time is the highest in the case of the HadGEM2-CC (0.752 and 0.748). On the one hand, the ACCESS1-3 simulation results in the closest average value of the standard deviation (0.067 in both cases) to the ERA-20C (0.069 and 0.067). On the other hand, ACCESS 1-3 show weaker correlation with ERA-20C than HadGEM2-CC. The model family MPI-ESM is characterized by similarly high correlation values as HadGEM2-CC, however, their standard deviations are smaller than the values of the ERA-20C.

Figure 3. Average values of spatial Pearson correlations (black straight lines), standard deviations (green semicircles) and centered root-mean-square differences (blue semicircles) on the basis of the strongest negative (a) Pearson correlations (b) Spearman correlations computed from the ERA-20C and the GCMs for the three time periods (1951-1980, 1961-1990, 1971-2000).

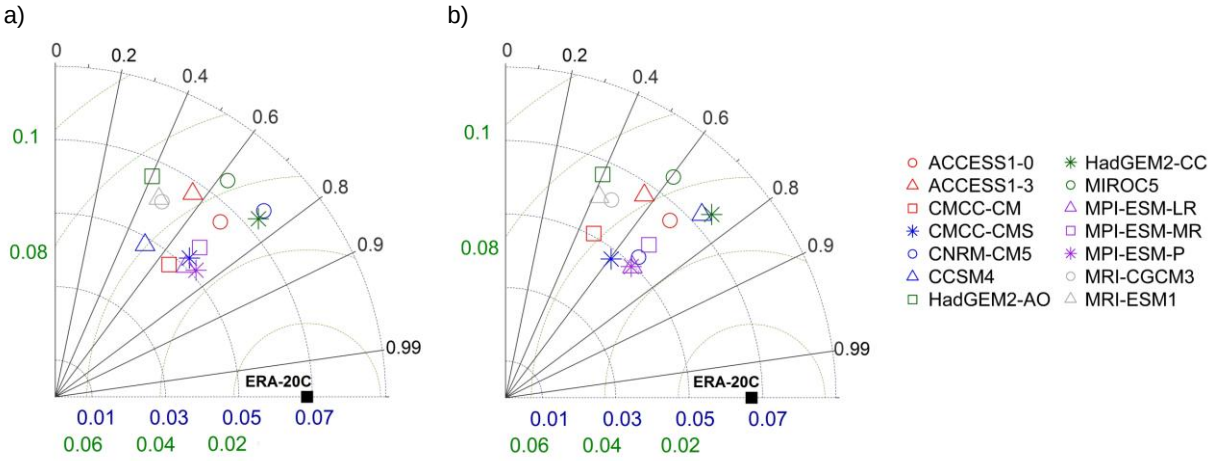

4.2. AT500hPa anomalies and 2m air temperature over the Carpathian Basin

After completing the analysis discussed in the section 4.1, the HadGEM2-CC can be chosen as the best-performing model. The location of the action centers representing the NAO and MO are summarized in *Table 3*.

Based on the action centers identified in the Pearson and Spearman correlation fields, AT500hPa anomalies are calculated and used as indices representing the teleconnection systems over the Northeast Atlantic and the Mediterranean region. After that, Pearson and Spearman correlation values between AT500hPa anomalies and near-surface air temperature datasets over the Carpathian Basin are computed in four cases regarding the NAO and MO, respectively. Figure 4 summarizes the results of the analysis. In the cases of a and c (b and d) AT500hPa anomalies are calculated over the Northeast Atlantic and the Mediterranean region based on Pearson (Spearman) correlations. In the cases of a and b (c and d) correlations are computed between AT500hPa anomalies and near-surface air temperature over the Carpathian Basin on the basis of Pearson (Spearman) correlations. A lag of one/two days was used concerning the MO/NAO. The application of these lags leads to the greater numbers of significant correlations in every examined cases above the Carpathian Basin.

Table 3. Location of the action centers in the HadGEM2-CC based on the strongest negative Pearson and Spearman correlations over the Northeast Atlantic and the Mediterranean region, and associated correlation values.

Action centers	Period of time	Location based on Pearson correlation	Location based on Spearman correlation	Pearson correlation	Spearman correlation
North-east Atlantic	1951-1980	26°N & 40°W - 52°N & 38°W	26°N & 40°W - 52°N & 34°W	-0.459	-0.458
	1961-1990	26°N & 36°W - 52°N & 30°W	24°N & 42°W - 50°N & 38°W	-0.427	-0.444
	1971-2000	28°N & 34°W - 54°N & 24°W	26°N & 34°W - 52°N & 28°W	-0.450	-0.451
Mediter-ranean	1951-1980	36°N & 2°E - 24°N & 26°E	36°N & 6°E - 24°N & 30°E	-0.441	-0.448
	1961-1990	34°N & 0°E - 22°N & 24°E	36°N & 2°W - 24°N & 24°E	-0.444	-0.440
	1971-2000	34°N & 2°E - 22°N & 26°E	34°N & 4°E - 22°N & 28°E	-0.436	-0.438

First, the number of grid points with significant correlations and their associated values are analyzed for the period of 1951-1980. Action centers are detected in the same position in the ERA-20C datasets regardless whether they are based on the Pearson or Spearman strongest negative correlations. The number of grid points with significant correlation values between AT500hPa anomalies and near-surface air temperature over the Carpathian Basin exceeds 50% of the total grid points in every cases regarding the MO. Their average values vary between 0.278 and 0.282. In the HadGEM2-CC, the number of grid points with significant correlation values concerning the NAO/MO are larger/smaller than those in the ERA-20C. It exceeds 50% only in the case of b and d regarding the MO. However, a slight overestimation of correlation are observed comparing to the ERA-20C (0.292 and 0.306).

If the 30-year-long period is shifted by one decade to 1961-1990, the number of grid points with significant correlation values in the ERA-20C increases over the Carpathian Basin concerning the NAO, however its spatial coverage exceeds 50% only in the case of d. Regarding the MO, the ratio of the grid points is over 50% in every cases. The average values of correlations are between 0.314 and 0.362, which means that the spatial variation increased relative to the period of 1951-1980. In the HadGEM2-CC fewer grid points can be found with significant correlations. The spatial coverage of significant correlation exceeds 50% only in the cases of b and d. The average values of correlations associated with these cases are 0.292 and 0.306, respectively. Consequently, HadGEM2-CC underestimates the correlation values computed on the basis of the ERA-20C.

Because of the detected eastward shift of the northern action center over the Northeast Atlantic, an increasing number of grid points with significant correlations and increasing correlation values are expected for the period of 1971-2000. In the ERA-20C the number of grid points over the Carpathian Basin exceeds 50% of all the grid points in the cases of a, b and c; in addition, every grid point can be considered significant in the case of d. Their average values vary between 0.262 and 0.268 concerning the four cases. Regarding the MO, every grid point in the cases of b, c and d can be considered significant over the Carpathian Basin with average values between 0.362 and 0.377. In the HadGEM2-CC, the number of grid points with significant correlations is over 50% in the cases of b, c and d. It reaches 100% in the case of a. It overestimates correlations substantially in the cases of a and c. Their average values vary between 0.270 and 0.324. This overestimation may be explained as follows. The oscillation phenomenon over the Northeast Atlantic is closer to the geographic latitude of the Carpathian Basin compared to the ERA-20C. Smaller number of significant correlation are found

concerning the MO and their associated correlation values are underestimated relative to the ERA-20C. The number of the grid points exceeds 50% only in the cases of b and d. Their average values are between 0.257 and 0.270. Results are shown in *Figure 5* for the period of 1971-2000.

Finally the distribution of grid points with significant correlations is analyzed. In the ERA-20C the distribution of the significant correlation values are similar over the Carpathian Basin in all the four cases listed above concerning both the NAO and MO. Regarding the NAO/MO, grid points with significant correlations are found over the southwestern/ northwestern part of the Carpathian Basin mostly. In general, HadGEM2-CC underestimates the number of grid points concerning the MO but their distributions follow similar pattern as in the ERA-20C regarding both the NAO and MO. The underestimation can be explained as follows. Despite stronger positive correlation in the case of the HadGEM2-CC, action centers over the Mediterranean region are located southerly compared to the ERA-20C.

Figure 4. Significant correlation values (>0.2) over the Carpathian Basin for the period of 1971-2000 in the ERA-20C. AT500hPa anomalies are calculated over (a-d) the Northeast Atlantic and (e-h) the Mediterranean region. AT500hPa anomalies are based on (a,c,e,g) Pearson correlations and (b,d,f,h) Spearman correlations. Between AT500hPa anomalies and near-surface air temperature (a-b, e-f) Pearson correlation values and (c-d, g-h) Spearman correlation values are computed.

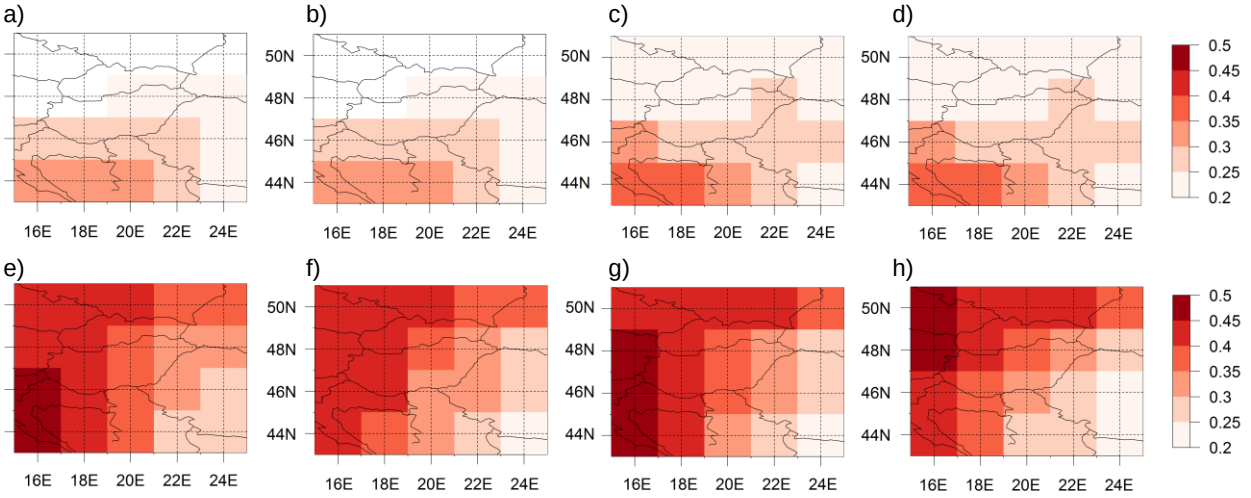

Figure 5. Significant correlation values (>0.2) over the Carpathian Basin for the period of 1971-2000 in the HadGEM2-CC. AT500hPa anomalies are calculated over (a-d) the Northeast Atlantic and (e-h) the Mediterranean region. AT500hPa anomalies are based on (a,c,e,g) Pearson correlations and (b,d,f,h) Spearman correlations. Between AT500hPa anomalies and near-surface air temperature (a-b,e-f) Pearson correlation values and (c-d,g-h) Spearman correlation values are computed.

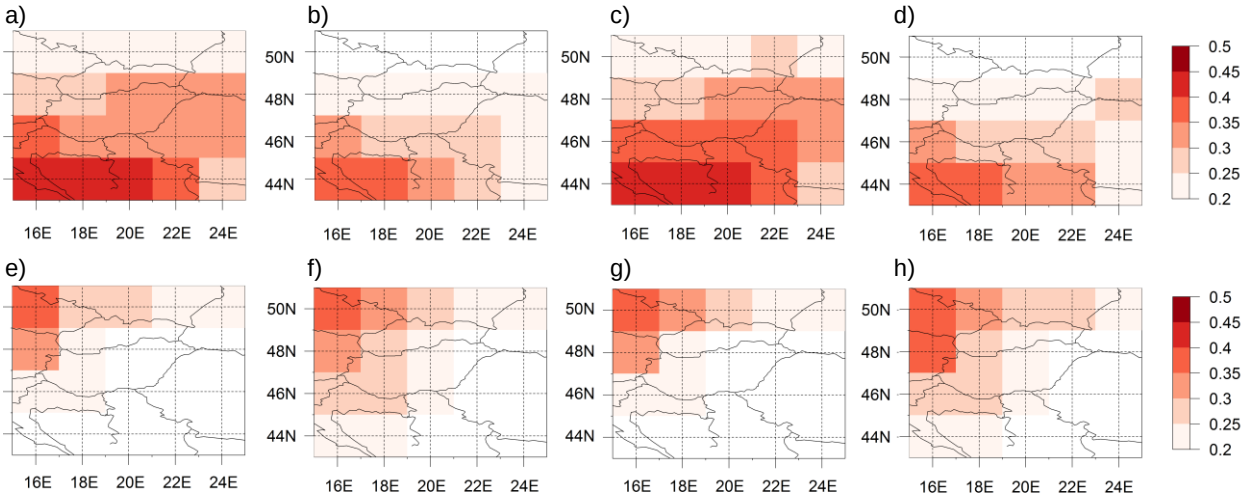

5. CONCLUSIONS

In this study oscillation phenomena (that may have significant effect on the near-surface temperature over the Carpathian Basin) were identified and analyzed on the basis of ERA-20C and GCM datasets. On the basis of the results presented here, the following conclusions can be drawn.

(1) Action centers of the teleconnection systems can be identified by applying statistical methods, e.g. identifying grid points associated with the strongest significant negative correlations in the ERA-20C and CMIP5 GCM datasets.

(2) Based on the identified pairs of grid points GCMs can be validated against the ERA-20C using model metrics. HadGEM2-CC was chosen as the best-performing model.

(3) Statistically significant connection is detected between AT500hPa and near-surface air temperature over the southwestern/western and northern part of the Carpathian Basin regarding the oscillation phenomena located over the Northeast Atlantic/Mediterranean region in the ERA-20C. In general, similarly distributed but weaker correlations can be found on the basis of the HadGEM2-CC than the ERA-20C concerning the MO.

Our ultimate goal is to apply more complex statistical methods to detect teleconnection systems that affect the Carpathian Basin and validate GCMs again. After the selection of the most reliable models, we aim to prepare improved predictions about the future climatic conditions of the Carpathian Basin throughout the 21st century.

Acknowledgements. Research leading to this paper has been supported by the following sources: the Ministry of National Development of the Hungarian Government via the AGRÁRKLIMA2 project (VKSZ_12-1-2013-0034), the Széchenyi 2020 programme, the European Regional Development Fund, and the Hungarian Government (GINOP-2.3.2-15-2016-00028), the Hungarian Scientific Research Fund under grants K-109109 and K-120605.

REFERENCES

American Meteorological Society (cited 2018): Teleconnection. Glossary of Meteorology. (Available online at http://glossary.ametsoc.org/wiki/Teleconnection.)

Barnston, AG, Livezey, RE (1987): Classification, Seasonality and Persistence of Low-Frequency Atmospheric Circulation Patterns. Monthly Weather Review, 115, 1083-1126.

Bartholy, J, Pongrácz, R, Geblyó, G (2010): Climate signals of the North Atlantic oscillation detected in the Carpathian basin. Applied Ecology and Environmental Research, 7, 229-240.

Bi, D, Dix, M, Marsland, SJ, O'Farrell, S, Rashid, HA, Uotila, P, Hirst, AC, Golebiewski, EKM, Sullivan, A, Yan, H, Hannah, N, Franklin, C, Sun, Z, Vohralik, P, Watterson, I, Zhou, Z, Fiedler, R, Collier, M, Ma, Y, Noonan, J, Stevens, L, Uhe, P, Zhu, H, Griffies, SM, Hill, R, Harris, C, and Puri, K (2013): The ACCESS coupled model: description, control climate and evaluation. Australian Meteorological and Oceanographic Journal, 63, 41–64.

Ciarlo, J, Aquilina, N (2015): An analysis of teleconnections in the Mediterranean region using RegCM4. International Journal of Climatology, 36, 797-808.

Climate Data Operators version 1.7.2 (Available at http://mpimet.mpg.de/cdo.)

Conte, M, Giuffrida, A, Tedesco, S (1989): The Mediterranean Oscillation: impact on precipitation and hydrology in Italy. Conference on Climate and Water, Publications of the Academy of Finland, Helsinki, 1, 121-137.

European Centre for Medium-Range Weather Forecasts (2014, updated daily): ERA-20C Project (ECMWF Atmospheric Reanalysis of the 20th Century). Research Data Archive at the National Center for Atmospheric Research, Computational and Information Systems Laboratory. (Available at https://doi.org/10.5065/D6VQ30QG.) Last accessed: 07.12.2017.

Gent, PR, Danabasoglu G, Donner, LJ, Holland, MM, Hunke, EC, Jayne, SR, Lawrence, DM, Neale, RB, Rasch, PJ, Vertenstein, M, Worley, PH, Yang, ZL, Zhang, M (2011): The Community Climate System Model version 4. Journal of Climate

Hurrell, J, Deser, C (2010): North Atlantic climate variability: The role of the North Atlantic Oscillation. Journal of Marine Systems, 79, 231-244.

Hurrell, JW, Kushnir, Y, Ottersen, G, Visbeck, M (2003): An Overview of the North Atlantic Oscillation, in The North Atlantic Oscillation: Climatic Significance and Environmental Impact (eds J. W. Hurrell, Y. Kushnir, G. Ottersen and M. Visbeck). American Geophysical Union, Washington, D. C.

Jung, T, Hilmer, M (2000): Evidence for a recent change in the link between the North Atlantic Oscillation and Arctic Sea ice export. Geophysical Research Letters, 27, 989-992.

Livezey, RE, Chen, WY (1983): Statistical Field Significance and its Determination by Monte Carlo Techniques. Monthly Weather Review, 111, 46-59.

R Core Team (2016). R: A language and environment for statistical computing. R Foundation for Statistical Computing, Vienna, Austria. (Available at https://www.R-project.org/.)

Scoccimarro, E, Gualdi, S, Bellucci, A, Sanna, A, Fogli, PG, Manzini, E, Vichi, M, Oddo, P, Navarra, A (2011): Effects of Tropical Cyclones on Ocean Heat Transport in a High Resolution Coupled General Circulation Model. Journal of Climate, 24, 4368-4384.

Stevens, B, Giorgetta, M, Esch, M, Mauritsen, T, Crueger, T, Rast, S, Salzmann, M, Schmidt, H, Bader, J, Block, K, Brokopf, R, Fast, I, Kinne, S, Kornblueh, L, Lohmann, U, Pincus, R, Reichler, T, Roeckner, E (2013): The Atmospheric Component of the MPI-M Earth System Model: ECHAM6. Journal of Advances in Modeling Earth Systems, 5. 146-172

Taylor, K, Stouffer, RJ, and Meehl, GA (2012): An overview of CMIP5 and the experiment design, Bulletin of the American Meteorological Society, 93, 485–498.

Taylor, KE (2001): Summarizing multiple aspects of model performance in a single diagram. Journal of Geophysical Research, 106, 7183-7192.

The HadGEM2 Development Team: Martin, GM, Bellouin, N, Collins, WJ, Culverwell, ID, Halloran, PR, Hardiman, SC, Hinton, TJ, Jones, CD, McDonald, RE, McLaren, AJ, O'Connor, FM, Roberts, MJ, Rodriguez, JM, Woodward, S, Best, MJ, Brooks, ME, Brown, AR, Butchart, N, Dearden, C, Derbyshire, SH, Dharssi, I, Doutriaux-Boucher, M, Edwards, JM, Falloon, PD, Gedney, N, Gray, LJ, Hewitt, HT, Hobson, M, Huddleston, MR, Hughes, J, Ineson, S, Ingram, WJ, James, PM, Johns, TC, Johnson, CE, Jones, A, Jones, CP, Joshi, MM, Keen, AB, Liddicoat, S, Lock, AP, Maidens, AV, Manners, JC, Milton, SF, Rae, JGL, Ridley, JK, Sellar, A, Senior, CA, Totterdell, IJ, Verhoef, A, Vidale, PL, Wiltshire, A (2011): The HadGEM2 family of Met Office Unified Model climate configurations. Geoscientific Model Development, 4, 723-757.

Voldoire, A, Sanchez-Gomez, E, Salas y Mélia, D, Decharme, B, Cassou, C, Sénési, S, Valcke, S, Beau, I, Alias, A, Chevallier, M, Déqué, M, Deshayes, J, Douville, H, Fernandez, E, Madec, G, Maisonnave, E, Moine, MP, Planton, S, Saint-Martin, D, Szopa, S, Tyteca, S, Alkama, R, Belamari, S, Braun, A, Coquart, L, Chauvin, F (2013): The CNRM-CM5.1 global climate model: description and basic evaluation. Climate Dynamics, vol. 40(9): 2091-2121.

Wallace, J, Gutzler, D (1987): Teleconnections in the Geopotential Height Field during the Northern Hemisphere Winter. Monthly Weather Review, 109, 784-812.

Watanabe, M, Suzuki, T, O'ishi, R, Komuro, Y, Watanabe, S, Emori, S, Takemura, T, Chikira, M, Ogura, T, Sekiguchi, M, Takata, K, Yamazaki, D, Yokohata, T, Nozawa, T, Hasumi, H, Tatebe, h, Kimoto, M (2010): Improved climate simulation by MIROC5: Mean states, variability, and climate sensitivity. Journal of Climate, 23, 6312-6335.

Yukimoto, S, Yoshimura, H, Hosaka, M, Sakami, T, Tsujino, H, Hirabara, M, Tanaka, TY, Deushi, M, Obata, A, Nakano, H, Adachi, Y, Shindo, E, Yabu, S, Ose, T, Kitoh, A (2011): Meteorological Research Institute-Earth System Model Version 1 (MRI-ESM1) – Model Description. Technical Report of the Meteorological Research Institute, 64, 83.